NANO LETTERS
Cite This: Nano Lett. 2019, 19, 8250−8254
Letter
pubs.acs.org/NanoLett

Large Anomalous Nernst Effect in a van der Waals Ferromagnet Fe_3GeTe_2

Jinsong Xu,*,† W. Adam Phelan,‡ and Chia-Ling Chien†

†Department of Physics and Astronomy, Johns Hopkins University, Baltimore, Maryland 21218, United States
‡Department of Chemistry, Johns Hopkins University, Baltimore, Maryland 21218, United States

Supporting Information

ABSTRACT: Anomalous Nernst effect, a result of charge current driven by temperature gradient, provides a probe of the topological nature of materials due to its sensitivity to the Berry curvature near the Fermi level. Fe_3GeTe_2, one important member of the recently discovered two-dimensional van der Waals magnetic materials, offers a unique platform for anomalous Nernst effect because of its metallic and topological nature. Here, we report the observation of large anomalous Nernst effect in Fe_3GeTe_2. The anomalous Hall angle and anomalous Nernst angle are about 0.07 and 0.09, respectively, far larger than those in common ferromagnets. By utilizing the Mott relation, these large angles indicate a large Berry curvature near the Fermi level, consistent with the recent proposal for Fe_3GeTe_2 as a topological nodal line semimetal candidate. Our work provides evidence of Fe_3GeTe_2 as a topological ferromagnet and demonstrates the feasibility of using two-dimensional magnetic materials and their band topology for spin caloritronics applications.

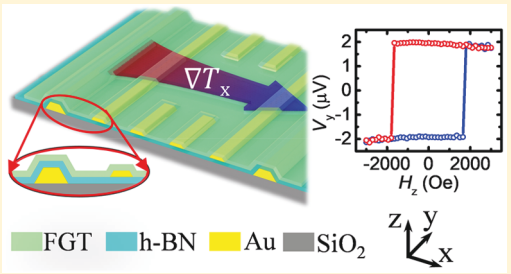

KEYWORDS: *anomalous Nernst effect, Fe_3GeTe_2, spin caloritronics, topological ferromagnet*

The recently discovered two-dimensional (2D) van der Waals (vdW) magnets,[1−8] providing new constituent materials for spintronics and caloritronics, have attracted much attention. To date, most 2D vdW ferromagnets are semiconductors (e.g., $Cr_2Ge_2Te_6$) and insulators (e.g., CrI_3), with Fe_3GeTe_2 (FGT) being the only ferromagnetic (FM) metal. Electrical switching of FGT by spin orbit torque[9,10] and tunneling magnetoresistance in FGT/h-BN/FGT heterostructure[11] have recently been demonstrated. FGT also has the highest Curie temperature (T_C) among the 2D vdW ferromagnets, and the value of T_C in thin FGT films can be tuned by ionic gating up to about room temperature.[3] Furthermore, the topological nature of FGT gives rise to some intriguing phenomena, for example, the observation of large anomalous Hall effect (AHE)[12] and magnetic skyrmions.[13−15] Of particular interest is the anomalous Nernst effect (ANE) in topological materials because the special band topology in these materials could introduce a very large ANE,[16−19] which shares some similarities with, but also differences from, the better known AHE. In AHE and ANE, the current is driven by an electric field and temperature gradient ∇T, respectively, while a voltage is measured perpendicular to both the current and the magnetization $\boldsymbol{M}$ of the material. While the AHE is dominated by the sum of the Berry curvatures for all the occupied states, ANE is determined by the Berry curvature at the Fermi level ε_F thus providing a different probe of the Berry curvature near ε_F and the topological nature of materials.[16−19] Therefore, FGT provides a unique platform for studying the ANE in 2D vdW ferromagnets and their topological properties.

In this work, we report the observation of AHE and ANE in exfoliated FGT thin film devices. We have determined σ_{xx}, defined as $\frac{\rho_{xx}}{\rho_{xx}^2+\rho_{xy}^2}$, and $\sigma_{xy}\left(-\frac{\rho_{xy}}{\rho_{xx}^2+\rho_{xy}^2}\right)$ the longitudinal and the transverse (or Hall) conductivities, respectively, as well as $S_{xx}\left(-\frac{\nabla V_x}{\nabla T_x}\right)$ and $S_{yx}\left(-\frac{\nabla V_y}{\nabla T_x}\right)$ the longitudinal and the transverse Seebeck coefficients, respectively. We have found very large AHE angle $\left(\theta_H=\frac{\sigma_{xy}}{\sigma_{xx}}\right)$ and very large ANE angle $\left(\theta_N=\frac{S_{yx}}{S_{xx}}\right)$, about 0.07 and 0.09 at low temperatures, respectively, much larger than those found in common FM metals of 0.02 or less[12,20−23] and comparable to those of other topological materials.[17,18,24] This places FGT outside the realm of common FM materials. We further found that the temperature dependence of the transverse thermoelectric conductivity α_{xy} follows the Mott relation $\alpha_{xy}=-\left(\frac{\pi^2k_B^2}{3e}\right)T\left(\frac{\partial\sigma_{xy}}{\partial\varepsilon}\right)_{\varepsilon_F}$, and the Hall resistivity follows the scaling relation of $\rho_{xy}=\lambda M\rho_{xx}^n$ with $n\approx 2$, where λ represents the strength of the spin−orbit coupling, M the magnetization, and ρ_{xx} (ρ_{xy}) the longitudinal (transverse) resistivity. This scaling relationship together with the observed large anomalous Hall conductivity (360−400 Ω^{-1} cm^{-1}) indicates

Received: September 10, 2019
Revised: September 27, 2019
Published: October 29, 2019

DOI: 10.1021/acs.nanolett.9b03739
Nano Lett. 2019, 19, 8250−8254

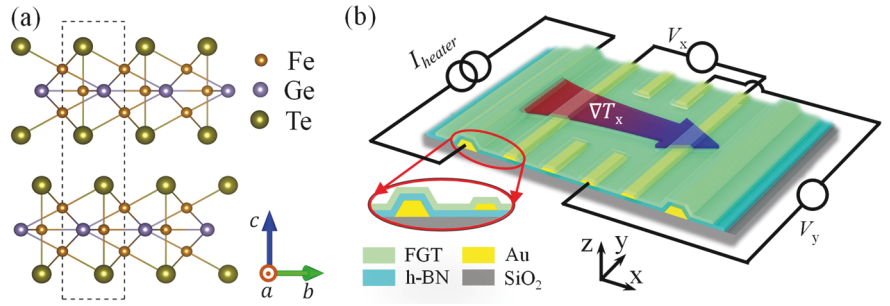

Figure 1. Crystal structure of Fe_3GeTe_2 (FGT) and FGT device for transport measurements. (a) Side view of Fe_3GeTe_2 crystal structure. Fe_3Ge slabs sandwiched by two layers of Te atoms and a van der Waals gap between the adjacent Te layers. The dashed rectangular box denotes the unit cell. (b) Fe_3GeTe_2 device structure for anomalous Nernst effect. A lateral temperature gradient ∇T_x is applied along the x direction, a magnetic field H_z is applied along the z direction, and both longitudinal and transverse voltages V_x and V_y are measured.

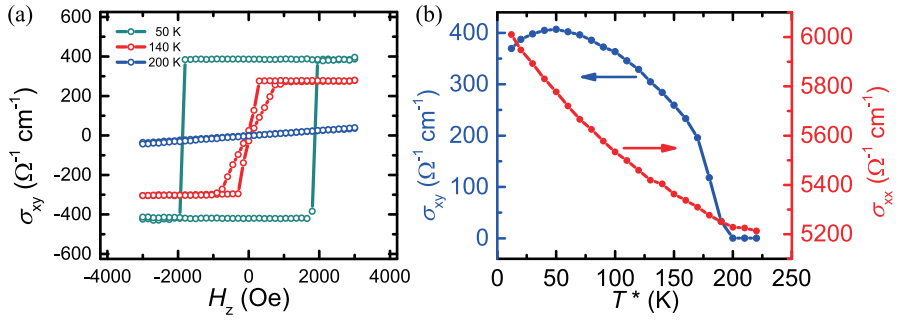

Figure 2. Temperature dependence of anomalous Hall effect (AHE). (a) Hall conductivity σ_{xy} as a function of external applied magnetic field H_z at different temperatures. (b) Temperature dependence of Hall conductivity σ_{xy} (blue curve) extrapolated at zero field and longitudinal conductivity σ_{xx} (red curve). σ_{xy} vanishes around 200 K, the Curie temperature T_C of the sample. The Hall angle $\theta_H = \frac{\sigma_{xy}}{\sigma_{xx}}$ reaches about 0.07 at low temperature.

the origin of the observed large AHE and ANE in FGT is primarily the intrinsic mechanism from the large Berry curvature, and not scattering, such as skew scattering and side-jump,[23,25,26] consistent with the topological nature of FGT.[12,27] Our work provides evidence for FGT as a topological ferromagnetic metal and demonstrates the feasibility of using 2D vdW magnetic materials and their band topology for spin caloritronic applications.

The vdW material of Fe_3GeTe_2 consists of Fe_3Ge slabs sandwiched by two layers of Te atoms and a van der Waals gap between the adjacent Te layers as shown in Figure 1a. Single crystals of bulk FGT, grown by chemical vapor transport method, exhibit a lattice constant of c = 16.36 Å, measured by X-ray diffraction (for details, see Supporting Information). The magnetic properties of bulk FGT, characterized by a superconducting quantum interference device, show a saturation magnetization of about 310 emu cm^{-3} with a magnetic moment of 1.25 μ_B per Fe atom and Curie temperature of about 200 K (see Supporting Information Figure S3). Thin FGT flake is mechanically exfoliated onto a heavily n-doped Si wafer with a 300 nm SiO_2 layer, then transferred onto prepatterned Au contacts using dry transferred method (see Supporting Information for details). The thickness of our FGT samples are about 20−40 nm. Figure 1b shows the schematic of a finished FGT device. There are two Au electrodes on the Si/SiO_2 substrate used as heaters to generate a lateral temperature gradient ∇T_x and also as a thermometer to measure the local temperature (see Supporting Information). There is a ∼20 nm h-BN insulating layer to electrically isolate the Au heaters and the FGT layer. On top of h-BN, there are Au electrodes to make electrical contact to the FGT layer to measure the longitudinal voltage V_x and transverse voltage V_y. For the measurements of both AHE and ANE, the magnetic field is applied out-of-plane, along the z-axis, unless otherwise noted.

We first examine the magnetic properties of FGT through the anomalous Hall effect with magnetometry results in the Supporting Information. For AHE, a small DC current (1 μA) is applied along the x-axis in FGT, while both longitudinal voltage V_x and transverse voltage V_y are measured. We experimentally measured the longitudinal (ρ_{xx}) and the transverse (ρ_{xy}) resistivities, which convert to $\sigma_{xx} = \frac{\rho_{xx}}{\rho_{xx}^2 + \rho_{xy}^2}$ and $\sigma_{xy} = -\frac{\rho_{xy}}{\rho_{xx}^2 + \rho_{xy}^2}$, the longitudinal and the transverse (or Hall) conductivities, respectively, for quasi 2D materials. As shown in Figure 2a, at low temperatures (50 K), the Hall conductivity σ_{xy} shows a rectangular hysteresis loop with sharp switching under an external magnetic field H_z, suggesting a single magnetic domain over the entire device. Together with the near 100% remnant σ_{xy} at zero field, these ferromagnetic hallmarks indicate that a thin FGT device exhibits strong perpendicular magnetic anisotropy (PMA) with the magnetic moments pointing in the out-of-plane direction. Thin films of common ferromagnets, hampered by the large shape anisotropy of $4\pi M$, rarely achieve PMA without very strong crystalline anisotropy or broken inversion symmetry and interface charge transfer. As the temperature increases (e.g., 140 K in Figure 2a), the rectangular hysteresis loop gradually evolves into narrow-waist shape due to the weakened PMA and the formation of a labyrinthine domain structure.[4] The temperature dependence of the Hall conductivity σ_{xy} extrapolated to 0 Oe and the longitudinal conductivity σ_{xx} is shown in Figure 2b. For increasing temperature, the value of

DOI: 10.1021/acs.nanolett.9b03739
Nano Lett. 2019, 19, 8250−8254

σ_{xy} decreases and vanishes around 200 K, similar to bulk single crystals of FGT. The longitudinal conductivity σ_{xx} varies about 10% within the measured temperature range. Very significantly, the Hall angle $\theta_H = \frac{\sigma_{xy}}{\sigma_{xx}}$ reaches about 0.07 at low temperatures, similar to previous reports,[12] much higher than those of common ferromagnets ($\lesssim$0.02).[20−23]

We next describe the anomalous Nernst effect results in thin FGT devices. As depicted in Figure 1b, by applying a DC current 14 mA to the right side heater, we generate an in-plane temperature gradient ∇T_x of about 1.3 K μm^{-1}. The transverse voltage V_y is measured as a function of external perpendicular magnetic field H_z as shown in Figure 3a. Similar to that of

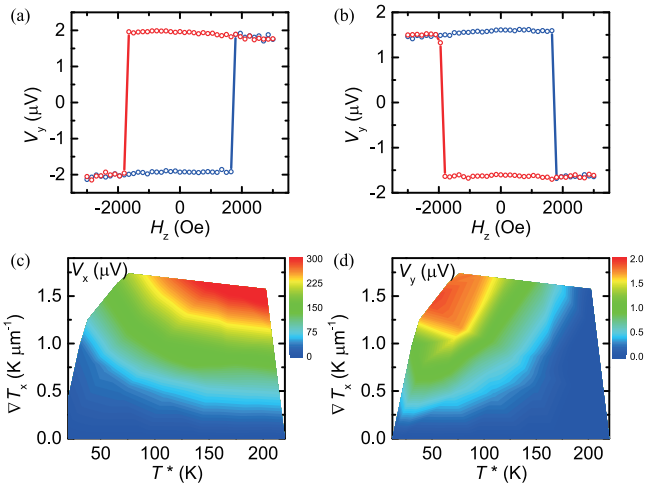

Figure 3. Anomalous Nernst effect (ANE), longitudinal voltage (V_x), and transverse voltage (V_y). (a) Nernst signal V_y as a function of H_z at ∇T_x = 1.3K μm^{-1}. (b) Nernst signal V_y as a function of H_z at ∇T_x = −1.1 K μm^{-1}. The data are taken at an effective sample temperature T^* = 45 K. The blue (red) curve is for increasing (decreasing) magnetic field. (c) Longitudinal voltage V_x (displayed in colors) as a function of temperature and temperature gradient. (d) Transverse voltage V_y (displayed in colors) as a function of temperature and temperature gradient. By definition, $\nabla V_x = -S_{xx}\nabla T_x$ and $\nabla V_y = -S_{yx}\nabla T_x$, both V_x and V_y will increase as a function of ∇T_x. The general trend that V_x (V_y) increases (then decreases) as T^* increases indicates S_{xx} (S_{yx}) increases (then decreases) with sample temperature T^*.

AHE, we observe a rectangular hysteretic ANE loop. When we apply 12 mA current to the left side heater to generate an opposite temperature gradient ∇T_x of about −1.1 K μm^{-1}, we observe a similar but reversed rectangular hysteresis loop as shown in Figure 3b. These results conclusively demonstrate ANE in the FGT device after we address one experimental issue. It is well-known that for thin films on thick substrates, the intended in-plane temperature gradient (∇T_x) is often accompanied inadvertently by an out-of-plane temperature gradient (∇T_z) due to the thermal conduction through the much thicker substrate. The latter may contribute an ANE voltage via $\nabla T_z \times M_x$, e.g., in permalloy thin films on Si substrate,[20] where permalloy has in-plane magnetization M_x. To assess and eliminate this possible contribution, we apply a large magnetic field H_x up to 6 kOe along the x direction and observed no appreciable signal (see Supporting Information Figure S5). This is because the PMA of FGT is so strong that there is no measurable M_x even with the presence of a large in-plane magnetic field. Thus, all the measured thermal voltage is due to the anomalous Nernst signal of $\nabla T_x \times M_z$ in FGT.

To gain further insight and extract the Seebeck coefficients at zero field, provided by the robust PMA, we measure the ANE in the FGT devices at different temperatures T^*, and also with different temperature gradients ∇T_x, as summarized in Figure 3c,d. The longitudinal voltage V_x and the transverse voltage V_y are displayed in colors as a function of T^* and ∇T_x. Using the definitions of $S_{xx} = -\nabla V_x/\nabla T_x$ and $S_{yx} = -\nabla V_y/\nabla T_x$, we obtain the ANE angle $\theta_N = \frac{S_{yx}}{S_{xx}}$ via LV_y/WV_x, where L = 10 μm and W = 5 μm are the length and width of the sample, respectively. We obtained very large ANE angle θ_N of as much as 0.09 at low temperature, a value much higher than those of common ferromagnets (<0.02).[20,21] These large ANE angle θ_N of 0.09 corroborates with the similarly large AHE angle θ_H of 0.07, both are much larger than those in common FM metals of $\lesssim$0.02 and comparable to those of other topological materials[17,18,20,24] (see Supporting Information Figure S6). Furthermore, while only Berry curvature near the Fermi level contributes to ANE, AHE originates from all the occupied bands. Therefore, these similar values of AHE and ANE angles may suggest the dominant contribution of a large Berry curvature near ε_F to AHE over all the other occupied bands in Fe_3GeTe_2.

With the measured longitudinal (S_{xx}) and transverse (S_{yx}) Seebeck coefficients, we can obtain the transverse thermoelectric conductivity $-\alpha_{xy}$. The temperature dependence of the transverse and longitudinal Seebeck coefficient S_{yx} and S_{xx} is shown in Figure 4a. The laws of thermodynamics and FM

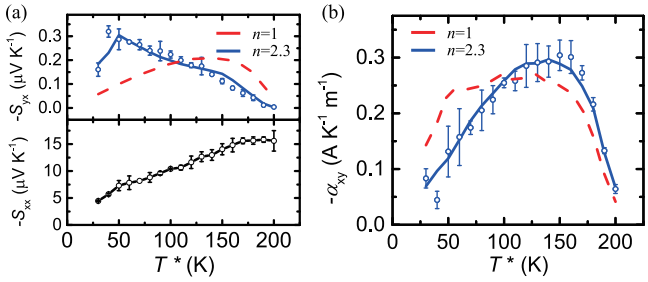

Figure 4. Temperature dependence of S_{yx}, S_{xx}, and α_{xy}. (a) Temperature dependence of S_{yx} (top panel) and S_{xx} (bottom panel). S_{xx} and S_{yx} is extracted from linear fitting V_x and V_y vs ∇T_x, respectively. (b) Temperature dependence of α_{xy}. α_{xy} is determined via eq 1. Blue solid curve is the best fit using eqs 2 and 3 for S_{yx} and α_{xy}, respectively, and red dashed curve is the best fit with n = 1.

ordering dictate the temperature dependence of S_{yx}, which must vanish at T = 0 K, remain finite below T_C, and become negligible above T_C. With the aid of the Mott relation,[16,23,28] quantitative analysis can be performed. The transverse thermoelectric conductivity $-\alpha_{xy}$ and Seebeck coefficients are related through

$$\alpha_{xy} = \sigma_{xx}S_{xy} + \sigma_{xy}S_{xx} = -\sigma_{xx}S_{yx} + \sigma_{xy}S_{xx} \quad (1)$$

Therefore, α_{xy} can be determined from the measured σ_{xx}, σ_{xy}, S_{xx}, and S_{yx}. However, if the Mott relation holds, α_{xy} can be obtained from via $\alpha_{xy} = -\left(\frac{\pi^2 k_B^2}{3e}\right) T \left(\frac{\partial \sigma_{xy}}{\partial \varepsilon}\right)_{\varepsilon_F}$, and S_{xx} from $S_{xx} = -\left(\frac{\pi^2 k_B^2}{3e}\right) T \left(\frac{\partial \ln \sigma_{xx}}{\partial \varepsilon}\right)_{\varepsilon_F}$, where k_B is the Boltzmann

DOI: 10.1021/acs.nanolett.9b03739
Nano Lett. 2019, 19, 8250−8254

constant, ε is the energy, and ε_F is the Fermi energy. By substituting the scaling relationship for the Hall resistivity $\rho_{xy} = \lambda M \rho_{xx}^{n}$ into the Mott relation and eq 1, we have[20,29]

$$S_{yx} = \frac{\sigma_{xy}}{\sigma_{xx}}\left(\left(\frac{\pi^2 k_B^2}{3e}\right)\frac{\left(\frac{\partial\lambda}{\partial\varepsilon}\right)_{\varepsilon_F}}{\lambda}T + (n-1)S_{xx}\right) \quad (2)$$

$$\alpha_{xy} = -\sigma_{xy}\left(\left(\frac{\pi^2 k_B^2}{3e}\right)\frac{\left(\frac{\partial\lambda}{\partial\varepsilon}\right)_{\varepsilon_F}}{\lambda}T + (n-2)S_{xx}\right) \quad (3)$$

To examine the Mott relation and determine the exponent n, we use eqs 2 and 3 to fit S_{yx} and α_{xy} to search for the best-fit values of $\frac{\left(\frac{\partial\lambda}{\partial\varepsilon}\right)_{\varepsilon_F}}{\lambda}$ and n, as shown in Figure 4. The best-fit exponent is $n = 2.3 \pm 0.1$ (blue solid curves). The exponent is clearly close to $n = 2$, and not $n = 1$, as shown in Figure 4. The scaling relationship with $n = 2$ indicates that the intrinsic mechanism or side-jump, instead of skew scattering, dominates AHE and ANE in FGT.[23,25,26] Previous reports have shown the intrinsic mechanism dominates AHE in FGT;[12,27] therefore, n close to 2 favors the intrinsic mechanism in FGT. At the same time, the anomalous Hall conductivity is $\sigma_{xy} \approx 360-400\ \Omega^{-1}\ cm^{-1}$ at low temperature, which is close to the intrinsic contribution $\sigma_{xy,in} \approx \frac{e^2}{ha_z} \approx 470\ \Omega^{-1}\ cm^{-1}$, where h is Planck constant and a_z is the interlayer distance ($a_z = c/2 = 8.18$ Å).[12,25−27] This further corroborates the intrinsic Berry curvature as the primary source of the observed large AHE and ANE angles. This is consistent with the recent proposal of FGT as a topological nodal line semimetal with a large Berry curvature from the nodal line.[12] This may be the reason for the exceptionally large AHE angle θ_H and ANE angle θ_N of 0.07 and 0.09, far larger than those in common ferromagnets.

In summary, we have observed ANE in exfoliated 2D van der Waals ferromagnetic metallic Fe_3GeTe_2 thin film devices. We have observed an exceptionally large anomalous Nernst effect angle θ_N of 0.09, corroborated by the similarly large anomalous Hall effect angle θ_H of 0.07, much larger than the values of ≤0.02 for common ferromagnetic metals. From the measured transport coefficients and the Mott relation, we find the large Berry curvature is responsible for the observed large AHE and ANE angles, which provides evidence for FGT as a topological ferromagnet. Our results demonstrate the feasibility of using 2D vdW magnetic materials and their band topology for spin caloritronics applications.

■ ASSOCIATED CONTENT

Supporting Information

The Supporting Information is available free of charge on the ACS Publications website at DOI: 10.1021/acs.nanolett.9b03739.

Description of device fabrication, Fe_3GeTe_2 bulk crystal growth and characterization, temperature calibration, and anomalous Nernst contribution from vertical temperature gradient (PDF)

■ AUTHOR INFORMATION

Corresponding Author

*E-mail: jxu94@jhu.edu.

ORCID

Jinsong Xu: 0000-0001-6035-7085

Author Contributions

J.X. and C.L.C. conceived the experiment. W.A.P. synthesized the bulk crystals. J.X. performed the experiment. J.X. and C.L.C. wrote the manuscript with the input from all authors. All the authors discussed the results.

Notes

The authors declare no competing financial interest.

■ ACKNOWLEDGMENTS

This work was supported by the National Science Foundation under grant DMREF-1729555. The bulk crystals were grown in the Platform for the Accelerated Realization, Analysis, and Discovery of Interface Materials (PARADIM) facilities supported by the National Science Foundation under Cooperative Agreement No. DMR-1539918.

■ REFERENCES

(1) Huang, B.; Clark, G.; Navarro-Moratalla, E.; Klein, D. R.; Cheng, R.; Seyler, K. L.; Zhong, D.; Schmidgall, E.; McGuire, M. A.; Cobden, D. H.; Yao, W.; Xiao, D.; Jarillo-Herrero, P.; Xu, X. Layer-dependent ferromagnetism in a van der Waals crystal down to the monolayer limit. *Nature* **2017**, *546*, 270.

(2) Gong, C.; Li, L.; Li, Z.; Ji, H.; Stern, A.; Xia, Y.; Cao, T.; Bao, W.; Wang, C.; Wang, Y.; Qiu, Z. Q.; Cava, R. J.; Louie, S. G.; Xia, J.; Zhang, X. Discovery of intrinsic ferromagnetism in two-dimensional van der Waals crystals. *Nature* **2017**, *546*, 265.

(3) Deng, Y.; Yu, Y.; Song, Y.; Zhang, J.; Wang, N. Z.; Sun, Z.; Yi, Y.; Wu, Y. Z.; Wu, S.; Zhu, J.; Wang, J.; Chen, X. H.; Zhang, Y. Gate-tunable room-temperature ferromagnetism in two-dimensional Fe_3GeTe_2. *Nature* **2018**, *563*, 94.

(4) Fei, Z.; Huang, B.; Malinowski, P.; Wang, W.; Song, T.; Sanchez, J.; Yao, W.; Xiao, D.; Zhu, X.; May, A. F.; Wu, W.; Cobden, D. H.; Chu, J.-H.; Xu, X. Two-dimensional itinerant ferromagnetism in atomically thin Fe_3GeTe_2. *Nat. Mater.* **2018**, *17*, 778.

(5) O'Hara, D. J.; Zhu, T.; Trout, A. H.; Ahmed, A. S.; Luo, Y. K.; Lee, C. H.; Brenner, M. R.; Rajan, S.; Gupta, J. A.; McComb, D. W.; Kawakami, R. K. Room temperature intrinsic ferromagnetism in epitaxial manganese selenide films in the monolayer limit. *Nano Lett.* **2018**, *18*, 3125.

(6) Bonilla, M.; Kolekar, S.; Ma, Y.; Diaz, H. C.; Kalappattil, V.; Das, R.; Eggers, T.; Gutierrez, H. R.; Phan, M.-H.; Batzill, M. Strong room-temperature ferromagnetism in VSe_2 monolayers on van der Waals substrates. *Nat. Nanotechnol.* **2018**, *13*, 289.

(7) Gibertini, M.; Koperski, M.; Morpurgo, A. F.; Novoselov, K. S. Magnetic 2D materials and heterostructures. *Nat. Nanotechnol.* **2019**, *14*, 408.

(8) Gong, C.; Zhang, X. Two-dimensional magnetic crystals and emergent heterostructure devices. *Science* **2019**, *363*, 706.

(9) Alghamdi, M.; Lohmann, M.; Li, J.; Jothi, P. R.; Shao, Q.; Aldosary, M.; Su, T.; Fokwa, B. P. T.; Shi, J. Highly efficient spin-orbit torque and switching of layered ferromagnet Fe_3GeTe_2. *Nano Lett.* **2019**, *19*, 4400.

(10) Wang, X., Tang, J., Xia, X., He, C., Zhang, J., Liu, Y., Wan, C., Fang, C., Guo, C., Yang, W., Guang, Y., Zhang, X., Xu, H., Wei, J., Liao, M., Lu, X., Feng, J., Li, X., Peng, Y., Wei, H., Yang, R., Shi, D., Zhang, X., Han, Z., Zhang, Z., Zhang, G., Yu, G.; Han, X. Current-driven magnetization switching in a van der Waals ferromagnet Fe_3GeTe_2. *arXiv:1902.05794*, **2019**.

(11) Wang, Z.; Sapkota, D.; Taniguchi, T.; Watanabe, K.; Mandrus, D.; Morpurgo, A. F. Tunneling spin valves based on Fe_3GeTe_2/hBN/Fe_3GeTe_2 van der Waals heterostructures. *Nano Lett.* **2018**, *18*, 4303.

(12) Kim, K.; Seo, J.; Lee, E.; Ko, K.-T.; Kim, B. S.; Jang, B. G.; Ok, J. M.; Lee, J.; Jo, Y. J.; Kang, W.; Shim, J. H.; Kim, C.; Yeom, H. W.; Min, B. I.; Yang, B.-J.; Kim, J. S. Large anomalous Hall current

DOI: 10.1021/acs.nanolett.9b03739
Nano Lett. 2019, 19, 8250−8254

induced by topological nodal lines in a ferromagnetic van der Waals semimetal. *Nat. Mater.* **2018**, *17*, 794.
(13) Park, T.-E., Peng, L., Zhang, X., Kim, S. J., Song, K. M., Kim, K., Weigand, M., Schütz, G., Finizio, S., Raabe, J., Xia, J., Zhou, Y., Ezawa, M., Liu, X., Chang, J., Koo, H. C., Kim, Y. D., Yu, X.; Woo, S. Observation of magnetic skyrmion crystals in a van der Waals ferromagnet Fe_3GeTe_2. *arXiv:1907.01425*, **2019**.
(14) Wu, Y., Zhang, S., Zhang, J., Wang, W., Zhu, Y. L., Hu, J., Wong, K., Fang, C., Wan, C., Han, X., Shao, Q., Taniguchi, T., Watanabe, K., Mao, Z., Zhang, X.; Wang, K. L. Néel-type skyrmion in WTe_2/Fe_3GeTe_2 van der Waals heterostructure. *arXiv:1907.11349*, **2019**.
(15) Wang, H., Wang, C., Zhu, Y., Li, Z.-A., Zhang, H., Tian, H., Shi, Y., Yang, H.; Li, J. Direct observations of chiral spin textures in van der Waals magnet Fe_3GeTe_2 nanolayers. *arXiv:1907.08382*, **2019**.
(16) Xiao, D.; Yao, Y.; Fang, Z.; Niu, Q. Berry-phase effect in anomalous thermoelectric transport. *Phys. Rev. Lett.* **2006**, *97*, 026603.
(17) Ikhlas, M.; Tomita, T.; Koretsune, T.; Suzuki, M.-T.; Nishio-Hamane, D.; Arita, R.; Otani, Y.; Nakatsuji, S. Large anomalous Nernst effect at room temperature in a chiral antiferromagnet. *Nat. Phys.* **2017**, *13*, 1085.
(18) Sakai, A.; Mizuta, Y. P.; Nugroho, A. A.; Sihombing, R.; Koretsune, T.; Suzuki, M.-T.; Takemori, N.; Ishii, R.; Nishio-Hamane, D.; Arita, R.; Goswami, P.; Nakatsuji, S. Giant anomalous Nernst effect and quantum-critical scaling in a ferromagnetic semimetal. *Nat. Phys.* **2018**, *14*, 1119.
(19) Li, X.; Xu, L.; Ding, L.; Wang, J.; Shen, M.; Lu, X.; Zhu, Z.; Behnia, K. Anomalous Nernst and Righi-Leduc Effects in Mn_3Sn: Berry Curvature and Entropy Flow. *Phys. Rev. Lett.* **2017**, *119*, 056601.
(20) Chuang, T. C.; Su, P. L.; Wu, P. H.; Huang, S. Y. Enhancement of the anomalous Nernst effect in ferromagnetic thin films. *Phys. Rev. B: Condens. Matter Mater. Phys.* **2017**, *96*, 174406.
(21) Hasegawa, K.; Mizuguchi, M.; Sakuraba, Y.; Kamada, T.; Kojima, T.; Kubota, T.; Mizukami, S.; Miyazaki, T.; Takanashi, K. Material dependence of anomalous Nernst effect in perpendicularly magnetized ordered-alloy thin films. *Appl. Phys. Lett.* **2015**, *106*, 252405.
(22) Miyasato, T.; Abe, N.; Fujii, T.; Asamitsu, A.; Onoda, S.; Onose, Y.; Nagaosa, N.; Tokura, Y. Crossover behavior of the anomalous Hall effect and anomalous Nernst effect in itinerant ferromagnets. *Phys. Rev. Lett.* **2007**, *99*, 086602.
(23) Onoda, S.; Sugimoto, N.; Nagaosa, N. Quantum transport theory of anomalous electric, thermoelectric, and thermal Hall effects in ferromagnets. *Phys. Rev. B: Condens. Matter Mater. Phys.* **2008**, *77*, 165103.
(24) Shiomi, Y.; Kanazawa, N.; Shibata, K.; Onose, Y.; Tokura, Y. Topological Nernst effect in a three-dimensional skyrmion-lattice phase. *Phys. Rev. B: Condens. Matter Mater. Phys.* **2013**, *88*, 064409.
(25) Onoda, S.; Sugimoto, N.; Nagaosa, N. Intrinsic versus extrinsic anomalous Hall effect in ferromagnets. *Phys. Rev. Lett.* **2006**, *97*, 126602.
(26) Nagaosa, N.; Sinova, J.; Onoda, S.; MacDonald, A. H.; Ong, N. P. Anomalous hall effect. *Rev. Mod. Phys.* **2010**, *82*, 1539.
(27) Liu, Y.; Stavitski, E.; Attenkofer, K.; Petrovic, C. Anomalous Hall effect in the van der Waals bonded ferromagnet $Fe_{3-x}GeTe_2$. *Phys. Rev. B: Condens. Matter Mater. Phys.* **2018**, *97*, 165415.
(28) Cutler, M.; Mott, N. F. Observation of Anderson localization in an electron gas. *Phys. Rev.* **1969**, *181*, 1336.
(29) Pu, Y.; Chiba, D.; Matsukura, F.; Ohno, H.; Shi, J. Mott relation for anomalous Hall and Nernst effects in $Ga_{1-x}Mn_xAs$ ferromagnetic semiconductors. *Phys. Rev. Lett.* **2008**, *101*, 117208.

DOI: 10.1021/acs.nanolett.9b03739
Nano Lett. 2019, 19, 8250−8254